Modified Antipodal Vivaldi Antenna with Shaped Elliptical Corrugation for 1-18 GHz UWB Application

Muhammad Ahmad Ashraf [1,3], Khalid Jamil [2], A. R. Sebak [3,4], Mobeen Shoaib [2], Zeyad Alhekail [1], Majeed Alkanhal [1], and Saleh Alshebeili [1,3]

[1] Department of Electrical Engineering
[2] Prince Sultan Advanced Technology Research Institute
[3] KACST Technology Innovation Center in RFTONICS for the e-Society
King Saud University, Riyadh, 11421, Kingdom of Saudi Arabia
{mashraf, majeed, zeyad}@ksu.edu.sa, {mobeen.shoaib, khalid.jamil}@psatri.org.sa

[4] Electrical and Computer Engineering Department
Concordia University, Montreal, Canada
abdo@ece.concordia.ca

Abstract ─ We present two antipodal tapered slot antennas: one with elliptical strips termination and the other modified with elliptical shaped corrugations. Compared to the other, the corrugated antenna uses elliptical slots loading to improve the gain by up to 1.9 dB over operational bandwidth 0.8-18 GHz. It also improves the front to back lobe ratio. The simulated frequency and time domain results are in good agreement with measured performance of both antennas. Experimental results verify a fidelity factor greater than 0.86 for both antennas by transmitting 30ps (3-18 GHz) Ultra-Wideband (UWB) pulses.

Index Terms ─ Corrugated UWB antenna, fidelity factor, time domain, ultra-wideband.

I. INTRODUCTION

Recent years have seen a great interest in performance improvement of Tapered Slot Antenna (TSA) due to its lightweight structure, ease of fabrication, end-fire radiation and ultra-broadband characteristics [1-4]. For broadband systems, the candidate antenna performance is characterized both in frequency and time domain, in order to transmit very narrow pulses [5-7]. Printed TSAs find applications in phased/scanning array, millimeter wave, low cost radar and short-range communication systems.

Based upon their feeding mechanism, the Vivaldi tapered slot antennas are mainly classified into two different geometries: planar and antipodal [8-10]. For planar TSA, the Microstrip-to-Slotline (MSL) transition is employed as a feeding balun that limits the bandwidth over two octaves. Moreover, due to radiation losses, MSL transition causes pattern degradation at certain frequencies that reduces the antenna efficiency. To alleviate the problems caused by the MSL feeding mechanism, Langley, et al. [11] introduced an antipodal UWB feeding configuration using a balun comprising of a microstrip, a parallel stripline and a symmetric double-sided slotline.

The Antipodal Tapered Slot Antenna (ATSA) with dielectric director placed in the antenna aperture enhances the gain by focusing energy in the end-fire direction [12]. In this method, the antenna height and weight is compromised to improve the gain performance. In another method proposed in [13], the gain of ATSA is improved at the cost of increased substrate dimensions toward broadside. However, this method does not improve the gain at lower frequency range. On the other hand, corrugation configuration of ATSA mitigates the higher Side-Lobe-Levels (SLL), reduces backward radiations and increases the low frequency gain of broadband antennas without compromising the antenna dimensions [2,6,14].

The System Fidelity Factor (SFF) incorporates space, time and frequency domain characteristics

Submitted On: October 19, 2013
Accepted On: October 9, 2014

1054-4887 © 2015 ACES

of antenna system in one value. In [7], the transmission coefficient S_{21} is used to calculate the SFF. In this technique, a calibrated Vector Network Analyzer (VNA) sweeps from 3-12 GHz to transmit a pulse with Full Width Half Maximum (FWHM) equals to 60ps.

In this paper, we present comprehensive frequency and time domain simulations and experimental measurements to investigate the frequency domain characteristics and the fidelity factor of two ATSAs system: one with elliptical shaped fins termination and the other with elliptical shaped edge corrugation (ATSA-EC). It is observed that the ATSA-EC is improving lower frequency gain of proposed UWB spectrum. The size of ATSA-EC is not increased for gain improvement. We have presented the design of ATSAs with system fidelity factor greater than 0.86 for very narrow UWB pulse with FWHM equals to 30ps, that is two times less than the pulse width of 60ps presented in [7]. In order to obtain the proposed pulse width of very short duration, VNA is used to transmit a frequency sweep signal from 3-18 GHz through the designed antenna transmit receive systems. The Inverse Fast Fourier Transform (IFFT) of the received signal (S_{21}) gave the antenna time-domain response. A novel method for analyzing the broadband antenna in time domain was demonstrated by transmitting and receiving true time domain narrow pulses through proposed antenna system, generated by wideband arbitrary waveform generator (12 GSa/s AWG) and mixed-signal oscilloscope (50 GSa/s MSO).

Furthermore, we have presented a mathematical expression for designing the exponential curve of ground plane conductor required for antipodal feed mechanism. The proposed antennas with this antipodal feed exhibit reflection coefficient of less than -14 dB for a bandwidth of 1-18 GHz. Note, that the Federal Communication Commission (FCC) unlicensed UWB band is 3.1-10.6 GHz, therefore, this antenna design leaves a big margin at both frequency ends. We also experimentally verified broadside pattern symmetry for E- and H-plane, side-lobe levels and gain performance of the two antennas.

II. ANTENNA DESIGN

The antenna elements shown in Fig. 1 are travelling wave ATSAs developed on Rogers 5880 substrate having dielectric constant, ε_r=2.2 and thickness, h=1.574 mm. The size of each antenna is 160x120 mm^2. The ATSAs contain the strip conductors on both sides of substrate. In order to have impedance matching over a bandwidth of more than 10:1, the tapered slot is designed by following the guidelines in [15]. The ATSAs are loaded with elliptical shaped strip conductors as shown in Fig. 1. The exponential taper C_g is used for the ground in order to achieve broadband microstrip to parallel plate transition. The tapered curve C_g is defined as:

$$C_g = w_y - 1 + 0.1 w_y e^{\alpha w_x}, \quad (1)$$

where α is the rate of transition for exponential curve defined as the following:

$$\alpha = \frac{1}{1.92\, w_x} \ln\left(\frac{w_y + 0.1\, w_t}{0.1\, w_t}\right), \quad (2)$$

w_x is the x-directed length of curve with w_y and w_t being the y-directed initial and final points, respectively. The variation of impedance bandwidth and radiation characteristics against different geometrical parameters of proposed ATSAs are analysed by full-wave simulation software CST Microwave Studio [16]. Table 1 presents geometry of ATSA which results 182% impedance bandwidth with required radiation performance.

In order to improve the radiation characteristics, elliptical edge corrugations are applied to ATSA as shown in Fig. 1 (b). At each edge of the antenna Unequal Half Elliptical Slots (UHES) are loaded with the period, C_s=17 mm. The largest UHES having minor axis and major axis radii R_{s1}=15 mm and R_{s2}=8 mm, respectively, is placed at the centre of elliptical fin. Whereas, the major axis radii of other UHESs are decreased linearly by the factor C_r=0.7 having the constant ellipticity ratio e_r=0.533=R_{s2}/R_{s1}.

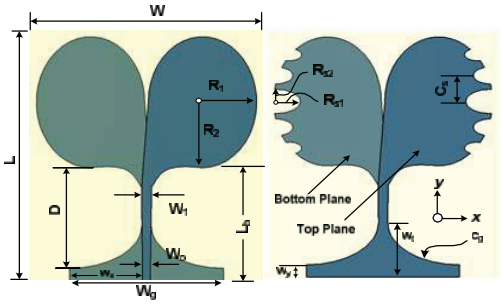

Fig. 1. Layout diagram of: (a) Antipodal Tapered Slot Antenna (ATSA) using elliptical shape loading, and (b) Antipodal Tapered Slot Antenna with elliptical shaped Edge Corrugation (ATSA-EC).

Table 1: Optimized geometrical dimensions (mm) of ATSAs

R_1	R_2	D	w_y	w_x	w_t	w_o	w_1
32.5	42.25	65	8	43.85	35	5.95	6.12

III. DISCUSSIONS AND REASONS

The photograph of fabricated ATSAs is shown in Fig. 2. The measured reflection coefficient of the corrugated fins and un-corrugated ATSAs are compared in Fig. 3. It can be seen that the performance of both antennas is comparable in terms of impedance bandwidth over a broad range of frequencies from 0.8-18 GHz. The reflection coefficient of designed ATSAs is better than 14 dB from 0.8 GHz to 18 GHz. Generally, the radiation of an ATSA is function of length, aperture width and substrate thickness. The added inductance due to edge corrugation increases the electrical length of antennas. The loading of ATSA with UHES can suppress the surface current at both back edges resulting in improved gain performance compared to un-slotted antenna gain. Similarly, the UHESs increase the effective length of the antenna resulting in more directive beams in both E- and H-planes.

Fig. 2. Photograph of fabricated ATSAs.

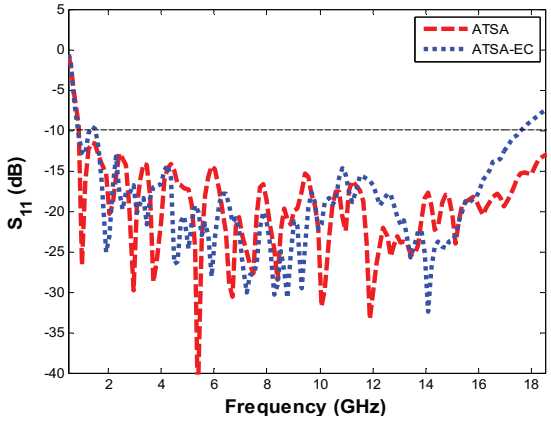

Fig. 3. Measured reflection coefficient characteristics of fabricated ATSAs.

A. Performance optimization

The performance of ATSAs against various corrugation depths is analysed by a parametric study using full wave simulations. From the parametric study the elliptical slots radii R_{s1} and R_{s2} are varied and gain performance is observed.

Figure 4 presents the simulation results of ATSAs gain performance against various corrugation depths compared to un-corrugated ATSA. The realized gain of ATSA is found between 3 dBi to 8.5 dBi over the 0.8 GHz to 6 GHz frequency band. The edge corrugation arranges the current path to be parallel with desired radiating current and opposite to the undesired surface current. The former enhances the gain, whereas, the later decreases the backward radiation. Therefore, the realized gain of ATSA-EC is improved over 0.8 GHz to 6 GHz band by varying elliptical slots radii R_{s1} and R_{s2}. Comparatively, better gain improvement is found for the ellipticity ratio $e_r=R_{s2}/R_{s2}$ less than 0.35 as depicted in Fig. 4 (a) and (b). It is worth noticing that the corrugated antenna has a stable gain performance near the lower and higher frequencies of the operating band.

Figure 5 presents the measured gain performance of fabricated prototypes from 2-18 GHz. The measured gain performances of both designs are in good agreement with simulation results, except at few frequencies with not more than ± 0.7 dB variations that may be due to fabrication tolerances regarding the top and bottom plane flair alignment and the cutting of elliptical strips for edge corrugation. Figure 5 (b) presents the results from 2 to 7 GHz to observe the

lower frequency gain improvement.

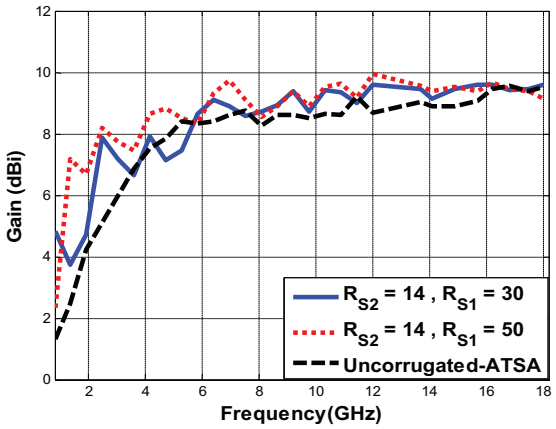

Fig. 4. Simulated gain characteristics of the ATSAs at different edge corrugation value.

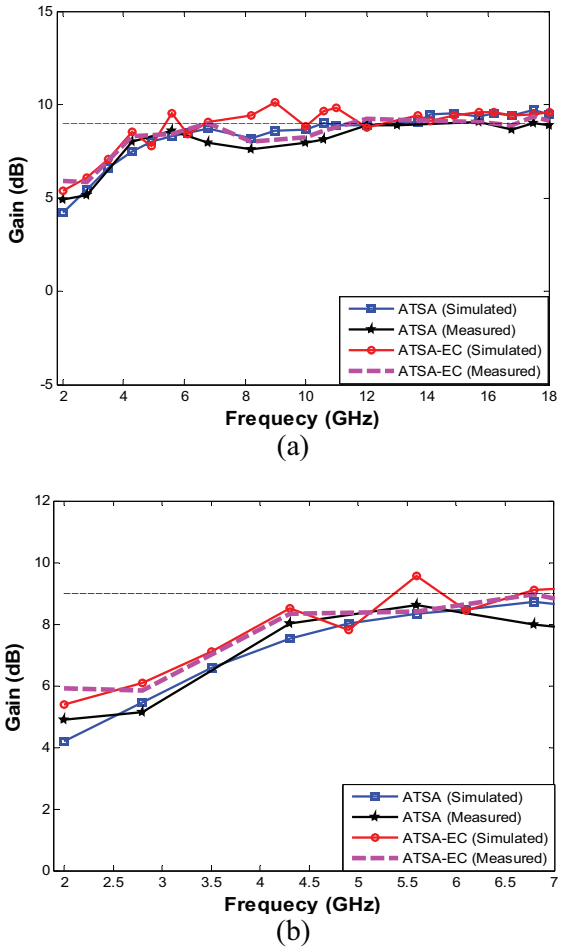

Fig. 5. Measured: (a) gain characteristics of the ATSAs, and (b) 2-7 GHZ.

B. Radiation analysis

The measured and simulated far field H-plane radiation patterns for the fabricated ATSAs prototype antennas are shown in Fig. 6 (a), (b) and (c) for frequencies 4.3, 8.2 and 16.8 GHz, respectively.

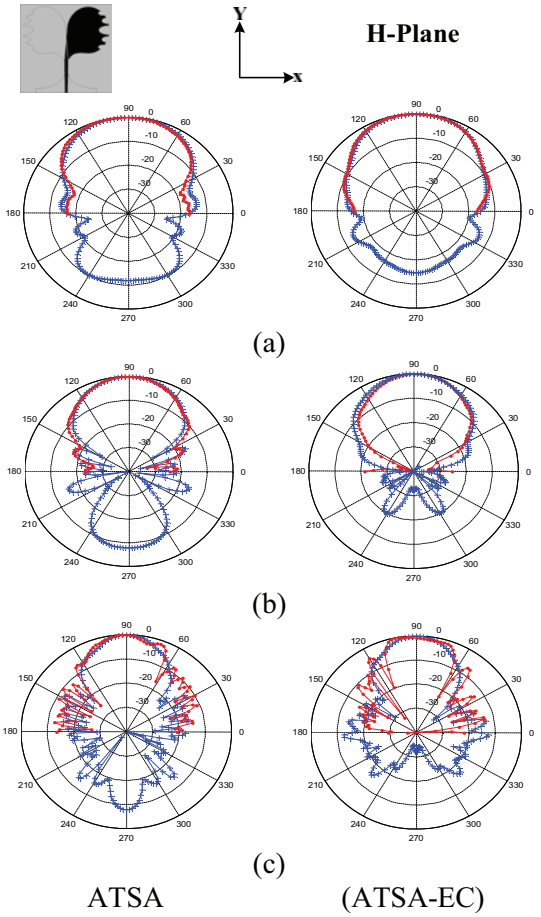

Fig. 6. H plane measured radiation patterns: (a) f=4.3 GHz, (b) f=8.2 GHz, and (c) f=16.8 GHz.

Similarly, the E-plane radiation patterns are presented in Fig. 7. The measured radiation patterns show good agreement with simulated patterns in both planes. The average 3-dB Half-Power Beam-Widths (HPBW) for the E-plane and H-plane patterns are 74° and 62°, respectively, with more than 10 dBi peak gain. The HPBW of the ATSA-EC in the H-plane is decreased to 46.9° from 56.7° at 8.2 GHz compared with ATSA. The change in E-plane beamwidth is not significant for both antennas.

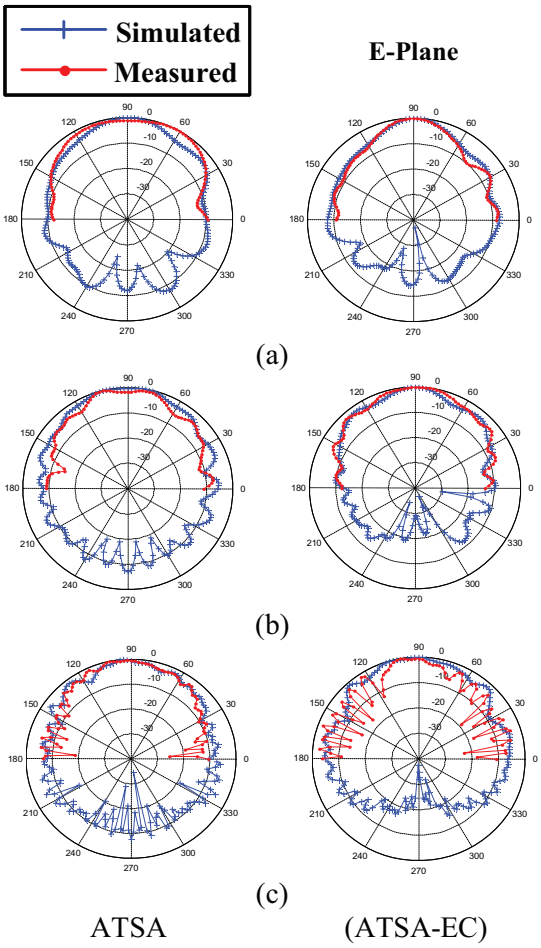

Fig. 7. E-plane measured radiation patterns: (a) f=4.3 GHz, (b) f=8.2 GHz, and (c) f=16.8 GHz.

In ATSAs currents are mainly distributed along the taper from the slot till the end of radiating element. Therefore, the maximum radiation is observed in the endfire direction. However, we have found undesired surface currents at the edges of elliptical conductors that contribute to radiating currents significantly beyond 9 GHz. An appropriate design of edge corrugation design is introduced to suppress these currents in order to reduce unwanted side lobes and back lobes resulting improvement in H-plane HPBW. Additionally, the SLL in the H-plane is significantly reduced by up to -10.2 dB from -7.2 dB for ATSA to -18.5 dB for ATSA-EC. The SLL in the E-plane is also improved by 4 dB at 8.2 GHz. The front-to-back ratio is also studied for different corrugation depths. The measured performance exhibits front-to-back ratio improvement by greater than 20 dB at certain frequencies.

C. Time domain analysis

The simulated time domain response of ATSAs when excited with passband Gaussian pulse covering the complete spectrum of operating frequency is shown in Fig. 8. The received pulses are obtained by placing an *x*-oriented *E*-field probe 10 m along the broadside direction of antenna. The FWHM of transmitted pulse is 30ps, while the received pulses preserve the Gaussian shape having maximum FWHM of 36ps related to ATSA-EC with R_{S1}=30 mm and R_{S2}=18 mm.

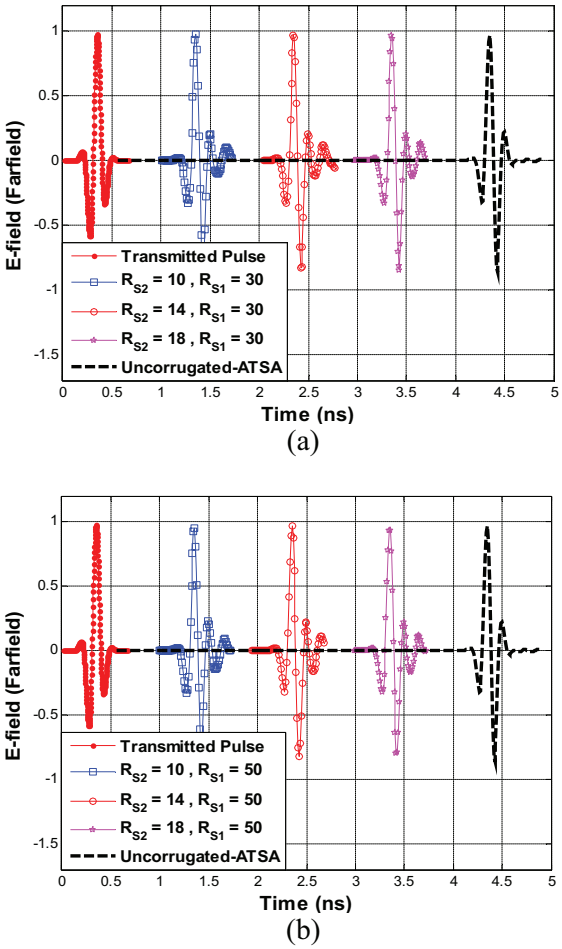

Fig. 8. Simulated transmitted and received pulses on the E-field probe for different edge corrugation parameters.

The FWHM of ATSA without corrugation and ATSA-EC with R_{S1}=50 and R_{S2}=14 is found 38ps and 39ps, respectively. The fidelity factor is calculated according to the following relation [17]:

$$Fidelity = \max_{\tau} \frac{\int_{-\infty}^{\infty} S_t(t) S_r(t-\tau) dt}{\sqrt{\int_{-\infty}^{\infty} |S_t(t)|^2 dt \, |S_r(t-\tau)|^2 dt}}, \quad (3)$$

where $S_t(t)$ and $S_r(t)$ present the transmitted and received time domain pulses, respectively. The fidelity factor for ATSA-EC at different edge corrugations is presented in Table 2.

Table 2: Calculated fidelity factor for ATSA-EC at different edge corrugation

$\frac{R_{s2}}{R_{s1}}$	10/30	14/30	18/30	10/50	14/50	18/50
Fidelity	0.89	0.88	0.87	0.91	0.92	0.9

D. Antenna system transfer function

Figure 9 presents the experimental setup for measuring the system transfer function $H(\omega)$ or S_{21} to characterize the ATSAs in time domain by IFFT. The system transfer function $H(\omega)$ is defined as the following:

$$H(\omega) = H_{TX}(\omega) H_{CH}(\omega) H_{RX}(\omega), \quad (4)$$

where $H_{TX}(w)$, $H_{CH}(w)$ and $H_{RX}(w)$ are the frequency domain transfer functions of the transmitting antenna, the channel and the receiving antenna, respectively. Two identical ATSAs are placed in front of each other at distance D=90 cm as shown in Fig. 9. The S_{21} amplitude and phase response is measured by using N5242A Vector Network Analyser (VNA) as shown in Fig. 10. In order to transmit a pulse without distortion, the S_{21} value should be constant over the desired frequency range.

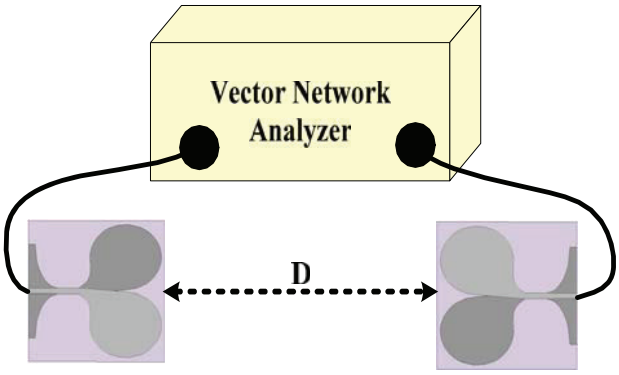

Fig. 9. Measurement Setup for time domain characteristics of ATSAs.

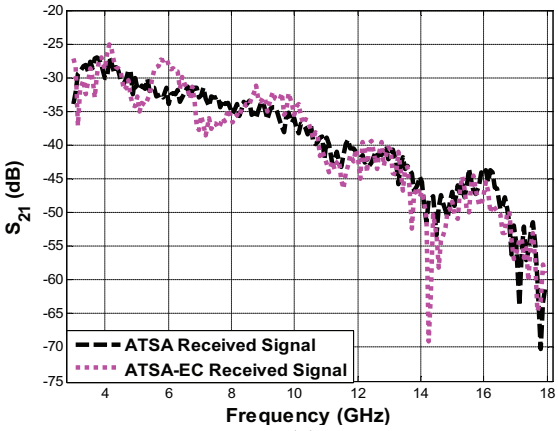

(a)

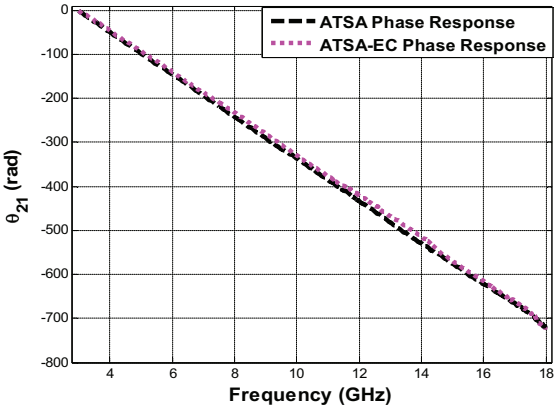

(b)

Fig. 10. Measured received: (a) signal response, and (b) phase response of ATSAs at D=90 cm.

E. Pulse distortion analysis

The magnitude (S_{21}) and phase response (θ_{21}) of antenna system is an important parameter for pulse distortion analysis. The distortion will be observed in the transmitted pulse, if the magnitude dip in S_{21} corresponds to nonlinearity in θ_{21} [7]. The magnitude response presented in Fig. 10 (a) shows linear characteristics over complete spectrum, except 14.2 GHz corresponds to lower antenna gain point. However, the phase response shown in Fig. 10 (b) is linear over the desired frequency band. The measured S_{21} parameter is then transformed into time domain by readily available analysis capability of VNA using IFFT.

In order to collect reliable data, a calibration is made from 3 GHz to 18 GHz with 800 points. The transformation from frequency to time domain is

accomplished by windowing the frequency domain data using Kaiser window with $\alpha=6$ [18]. The measured S_{21} data can be converted to time domain using the expression:

$$S_{21}(t) = sf \times IFFT\left[S_{21}(j\omega)w(n|\alpha=6)\right], \quad (5)$$

where *sf* is a scaling factor. A scaling factor of 2 is used for IFFT transformation of measured S_{21} [18]. The measured time domain response of the two antennas at D=90 cm is shown in Fig. 11. The transmitted pulse response is obtained by directly connecting both ports of the network analyser and applying IFFT to S_{21} value. The measured FWHM of transmitted pulse is 30ps. The calculated fidelity factor for ATSA and ATSA-EC is found to be 0.89 and 0.86, respectively. The FWHM of ATSA-EC is slightly greater than ATSA.

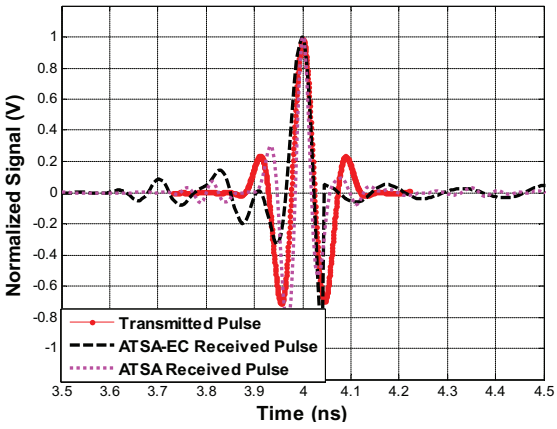

Fig. 11. Measured impulse response of the configuration shown in Fig. 9 with D=90 cm.

F. Experimental time-domain characterization

The accuracy of time domain analysis is further verified by sending true time domain pulses involving ATSA as pair of transmit and receives antennas. Figure 12 presents the experimental setup arrangement for characterization of antenna in time domain by sending UWB pulses generated by a wideband Arbitrary Waveform Generator (AWG). In this arrangement, the UWB signal is generated by M8190A 12GS/s AWG. It is then up-converted to 7 GHz using 8267D Vector Signal Generator (VSG) and transmitted via antenna. The output power of AWG is adjusted to 0 dBm. The output of VSG is divided into two paths by using 10 dB directional coupler. The Coupler's direct port (P_2) is connected to ATSA, whereas, the coupled output (P_3) is connected to four channel MSO72004 mixed signal oscilloscope. The coupled port output connected to oscilloscope is considered as reference signal, whereas, the couplers direct port output is transmitted and received by a pair of ATSA.

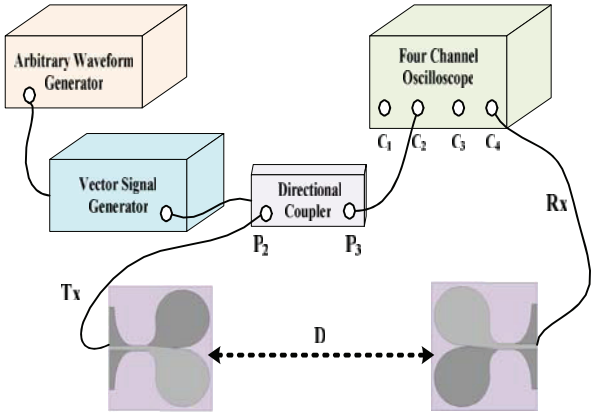

(a)

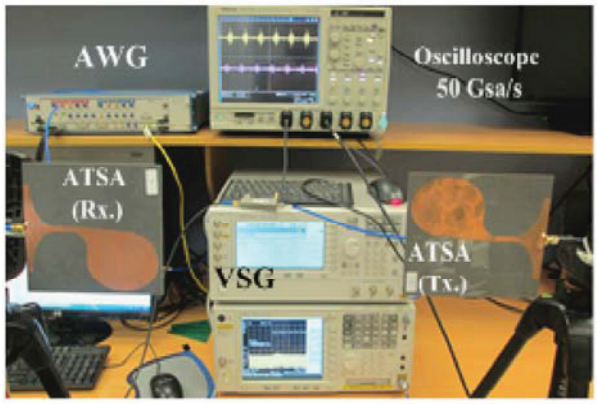

(b)

Fig. 12. Experimental setup for time domain measurement of ATSAs: (a) block diagram, and (b) photograph.

The time domain transmitted and Digitally Down Converted (DDC) received signals are shown in Fig. 13 (a). The corresponding up-converted signal with 7 GHz centre frequency is shown in Fig. 13 (b). The signal fidelity factor for transmitted signal $S_t(t)$ and received signal $S_r(t)$ is calculated by using eq. (3) and found 0.91, 0.897 at D=10 and 50 cm, respectively.

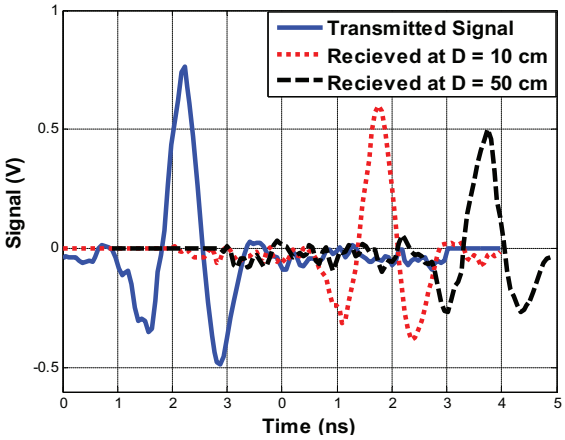

(a)

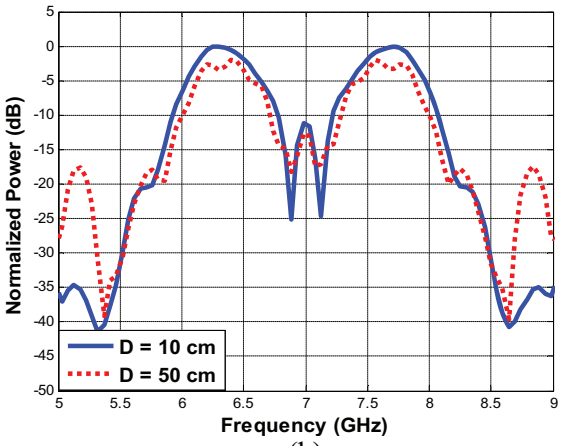

(b)

Fig. 13. Measured impulse response: (a) respected spectrum, and (b) of the configuration shown in figure at D=10cm and D=50 cm.

IV. CONCLUSION

We have presented the design of two antennas: Antipodal Tapered Slot Antenna (ATSA) and elliptical shaped Edge Corrugation (ATSA-EC). Both antennas find impedance bandwidth matched over 0.8-18 GHz corresponds to 182% fractional bandwidth. The effects of shaped elliptical corrugation on the antenna characteristics are: increase in electrical length due to added inductance which results in gain improvement at particular frequencies of proposed spectrum. Additionally, it reduces half power beamwidth and suppresses backward radiation which improves front to back ratio. The realised gain of ATSA-EC is improved up to 1.9 dB over 0.6-6 GHz band by varying the corrugation depths of elliptical shaped slots. ATSA-EC exhibits supressed back-lobe radiation up to 15 dB at higher frequencies of our proposed band. The radiation parameters and gain are optimized by the ellipticity ratio $e_r=R_{s2}/R_{s1}$ of corrugation slots. We have performed comprehensive frequency and time domain simulations and measurements to investigate impedance bandwidth, gain performance, radiation characteristics, and system transfer function and fidelity factor of antennas. For an ultra-short pulse having FWHM of 30ps, we have verified a fidelity factor greater than 0.86 for both antenna systems.

ACKNOWLEDGMENT

This research is supported by KACST Technology Innovation Center in Radio Frequency and Photonics for the e-Society.

REFERENCES

[1] L. A. Bui, A. Mitchell, K. Ghorbani, C. Tan-Huat, S. Mansoori, and E. R. Lopez, "Wide-band photonically phased array antenna using vector sum phase shifting approach," *IEEE Transactions on Antennas and Propagation*, vol. 53, no. 11, pp. 3589,3596, November 2005.

[2] L. S. Locke, J. Bornemann, and S. Claude, "Substrate integrated waveguide-fed tapered slot antenna with smooth performance characteristics over an ultra-wide bandwidth," *Applied Computational Electromagnetics Society Journal*, vol. 28, pp. 454-462, May 2013.

[3] T. Namas and M. Hasanovic, "Ultra-wideband antipodal vivaldi antenna for road surface scanner based on inverse scattering," *28th Annual Review of Progress in Applied Computational Electromagnetics (ACES)*, pp. 882-887, Monterey, CA, April 2012.

[4] S. Dai, L. Liu, and G. Fang, "A low-cost handheld integrated UWB radar for shallow underground detection," *2010 IEEE International Conference on Ultra-Wideband (ICUWB)*, vol. 2, pp. 1-4,September 2010.

[5] F. Fereidoony, S. Chamaani, and S. A. Mirtaheri, "UWB monopole antenna with stable radiation pattern and low transient distortion," *IEEE Antennas and Wireless Propagation Letters*, vol. 10, pp. 302,305, 2011.

[6] D. M. In, M. J. Lee, D. Kim, C. Y. Oh, and Y. S. Kim, "Antipodal linearly tapered slot antenna using unequal half-circular defected sides for gain improvements," *Microw. Opt. Technol. Lett.*, 54: pp. 1963-1965, May 16, 2012.

[7] G. Quintero, J. F. Zurcher, and A. K. Skriverviky, "System fidelity factor: a new method for comparing UWB antennas," *IEEE Transactions on*

Antennas and Propagation, vol. 59, no. 7, pp. 2502,2512, July 2011.

[8] Y. Che, K. Li, X. Hou, and W. Tian, "Simulation of a small sized antipodal vivaldi antenna for UWB applications," *2010 IEEE International Conference on Ultra-Wideband (ICUWB)*, vol. 1, pp. 1,3, September 20-23, 2010.

[9] K. Ebnabbasi, C. Rappaport, H. Foltz, and J. McLean, "Impulse response of vivaldi antenna using cubic-spline and exponential taper profiles for compact ground penetrating radar applications," *2010 IEEE Antennas and Propagation Society International Symposium (APSURSI)*, pp. 1,4, July 11-17, 2010.

[10] Y. J. Cheng, W. Hong, and K. Wu, "Design of a monopulse antenna using a dual V-type linearly tapered slot antenna (DVLTSA)," *IEEE Transactions on Antennas and Propagation*, vol. 56, no. 9, pp. 2903,2909, September 2008.

[11] J. D. S. Langley, P. S. Hall, and P. Newham, "Novel ultrawide-bandwidth vivaldi antenna with low cross-polarisation," *Electronics Letters*, vol. 29, no. 23, pp. 2004,2005, November 11, 1993.

[12] J. Bourqui, M. Okoniewski, and E. C. Fear, "Balanced antipodal vivaldi antenna with dielectric director for near-field microwave imaging," *IEEE Transactions on Antennas and Propagation*, vol. 58, no. 7, pp. 2318,2326, July 2010.

[13] K. Kota and L Shafai, "Gain and radiation pattern enhancement of balanced antipodal vivaldi antenna," *Electronics Letters*, vol. 47, no. 5, pp. 303,304, March 3, 2011.

[14] D. C. Chang, B. H. Zeng, and J. C. Liu, "Modified antipodal fermi antenna with piecewise-linear approximation and shaped comb corrugation for ranging applications," *IET Microwaves, Antennas & Propagation*, vol. 4, no. 3, pp. 399,407, March 2010.

[15] J. Y. Siddiqui, Y. M. M. Antar, A. P. Freundorfer, E. C. Smith, G. A. Morin, and T. Thayaparan, "Design of an ultra-wideband antipodal tapered slot antenna using elliptical strip conductors," *IEEE Antennas and Wireless Propagation Letters*, vol. 10, pp. 251-254, 2011.

[16] *CST-Computer Simulation Technology*, 2010.

[17] D. H. Kwon, "Effect of antenna gain and group delay variations on pulse-preserving capabilities of ultrawideband antennas," *IEEE Transactions on Antennas and Propagation*, vol. 54, no. 8, pp. 2208,2215, August 2006.

[18] S. Licul and W. A. Davis, "Unified frequency and time-domain antenna modeling and characterization," *IEEE Transactions on Antennas and Propagation*, vol. 53, no. 9, pp. 2882,2888, September 2005.

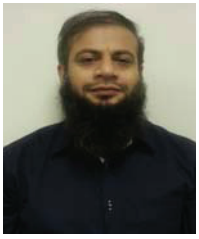

Muhammad Ahmad Ashraf received undergraduate education in Electrical Engineering from the University of Engineering and Technology (UET) Lahore in 2003. He received his M.S. degree in Microwave Engineering from National University of Sciences and Technology (NUST), Rawalpindi in 2009. He joined the Electrical Engineering Department, King Saud University (KSU), Riyadh where he received his Ph.D. degree in 2014. During his Ph.D. research, he was with Microwave, Antenna and Radar Systems (MARS) Laboratory at Prince Sultan Advanced Technology Research Institute (PSATRI), King Saud University. Currently he is working with the Technology Innovation Center, *RF and Photonics in the e-Society* (RFTONICS), funded by King Abdulaziz City for Science and Technology (KACST).

Abdel Sebak received the B.S. degree in Electronic and Communication Engineering from Cairo University, Egypt, in 1976, and in Applied Mathematics from Ain-Shams University, Egypt, in 1978. In 1980, he joined the Department of Electrical Engineering, University of Manitoba, Canada, where he obtained his M.Eng. and Ph.D. degrees in 1982 and 1984, respectively.

Sebak is a Professor with Concordia University. Before joining Concordia University, he was a Professor at the University of Manitoba and Cairo University. He was also with the Canadian Marconi Company, working on the design of microstrip phased array antennas.

Sebak's recent research activities cover two streams: Antenna Engineering, and Analytical and Computational Electromagnetics. Applied and sponsored projects include advanced composite materials for aerospace shielding and antenna applications, microwave sensing and imaging, ultra wideband and mm-wave antennas, microwave beamforming, and high gain mm-wave antennas.

Sebak is a Fellow of the Institute of Electrical and Electronics Engineers and Fellow of Engineering Institute of Canada. He is a Member of Concordia University Provost's Circle of Distinction for his career achievements.

Sebak is Co-Chair of IEEE ICUWB2015 and has served as Chair for the IEEE Canada Awards and Recognition Committee (2002-2004), IEEE Canada Conference Committee (2000-2002) and as the Technical Program Chair for the 2002 IEEE CCECE

Conference and the 2006 URSI-ANTEM Symposium. He has also served as a Member (2002-2004) of the IEEE RAB Awards and Recognition Committee. He is a Member of the Canadian National Committee of International Union of Radio Science (URSI) Commission B.

Mobien Shoaib received undergraduate education in Computer Engineering from National University of Sciences and Technology (NUST) in 2001. He received his M.S. degree in Telecommunication Engineering, from the Department of Electrical Engineering, Helsinki University of Technology (HUT), Espoo, Finland, in 2005. He was associated with the Department of Signal Processing and Acoustics at HUT until 2008. He is currently working in Signal and Image Processing Laboratory at Prince Sultan Advanced Technology Research Institute (PSATRI), King Saud University.

Majeed A. S. Alkanhal received the B.S. and M.S. degrees from King Saud University, Riyadh, Saudi Arabia, in 1984 and 1986, respectively, and the Ph.D. degree from Syracuse University, Syracuse, NY, in 1994, all in Electrical Engineering. He is presently a Professor and Chairman of the Electrical Engineering Department at King Saud University, Riyadh, Saudi Arabia. His research interests are in antennas and propagation, computational electromagnetics, and microwave engineering.

Saleh A Alshebeili is Professor and Chairman (2001-2005) of the Electrical Engineering Department, King Saud University. He has more than 20 years of teaching and research experience in the area of *communications* and *signal processing*. Alshebeili is Member of the Board of Directors of Prince Sultan Advanced Technologies Research Institute (PSATRI), the Vice President of PSATRI (2008-2011), the Director of Saudi-Telecom Research Chair (2008-2012), and the Director (2011-Present) of the Technology Innovation Center, *RF and Photonics in the e-Society* (RFTONICS), funded by King Abdulaziz City for Science and Technology (KACST). Alshebeili has been on the editorial board of *Journal* of *Engineering Sciences* of King Saud University (2009-2012). He has also an active involvement in the review process of a number of research journals, KACST general directorate grants programs, and national and international symposiums and conferences.